Inelastic Effects in the Study of ^{23}Na and ^{23}Mg†

R. O. Nelson
Duke University and Triangle Universities Nuclear Laboratory, Durham, North Carolina 27706, and North Carolina State University, Raleigh, North Carolina 27607

and

N. R. Roberson
Duke University and Triangle Universities Nuclear Laboratory, Durham, North Carolina 27706
(Received 11 August 1972)

14 states of ^{23}Na with excitation energies <5.6 MeV and their mirror states in ^{23}Mg have been studied with the ^{24}Mg$(d, ^3$He$)^{23}$Na and ^{24}Mg$(d, t)^{23}$Mg reactions with a bombarding energy of 21.1 MeV. Differential cross-section measurements indicated significant differences between established $l=2$ transitions and large cross sections for "j-forbidden" $\frac{7}{2}^+$ and $\frac{9}{2}^+$ states. Failure of a distorted-wave analysis to predict these anomalies suggested that inelastic effects should not be neglected. Calculations with the coupled-channel Born approximation (CCBA) have produced agreement with experiment and have shown that multiple-step processes not only dominate the transitions to the "j-forbidden" states, but have large effects upon allowed transitions as well. From the CCBA predictions it was possible to identify mirror states of the nuclei and to establish J^π assignments of $\frac{9}{2}^+$, $\frac{3}{2}^+$, $(\frac{5}{2}^+)$, $(\frac{5}{2}^-)$, $(\frac{7}{2}^+)$, $(\frac{5}{2}^+)$, and $(\frac{11}{2}^+)$ for the states in ^{23}Mg at 2.71, 2.90, 3.86, 3.97, 4.68, 5.29, and 5.45 MeV, respectively.

I. INTRODUCTION

The mirror nuclei ^{23}Na and ^{23}Mg have recently been subjects of considerable experimental and theoretical work. Studies of angular distributions for various nucleon-transfer reactions[1-5] and particle-γ angular correlations[6-10] revealed an energy spectrum for each nucleus that was reasonably well described by rotational bands built upon single-particle states of the Nilsson model. The observed spectroscopic factors and γ-decay properties for low-lying states were generally in fair agreement with the predictions of this collective model.

Recently, Poletti, Becker, and McDonald[8] extended spin and parity assignments in ^{23}Na to include all states below 5.8 MeV in excitation energy. However, the properties of some of the levels of ^{23}Mg remained uncertain. The present investigation was undertaken to study the higher levels of ^{23}Mg and ^{23}Na and to identify mirror states. Since the outset of this work, states in ^{23}Na have been studied further by nucleon-transfer reactions[11-13] and γ-ray decay measurements.[14-16] In addition McGrory and Wildenthal[17] have recently performed shell-model calculations for the mass-23 nuclei so that direct comparison of the two theories and experiment became possible.

The ^{24}Mg(d, t) and ^{24}Mg$(d, ^3$He$)$ reactions were chosen for this study, since transitions to states in both the ^{23}Mg and ^{23}Na nuclei could be studied simultaneously, and since the symmetry of the reactions would aid in the identification of mirror states. The angular-distribution measurements revealed striking differences in shape between established $l=2$ transitions and relatively large cross sections for the "j-forbidden" $\frac{7}{2}^+$ states. The usual distorted-wave Born approximation (DWBA) failed to predict these anomalies; this fact suggested that inelastic or multiple-step processes might be an important mechanism in these reactions. Such processes are likely to be enhanced due to the collective nature of ^{24}Mg. Predictions of a coupled-channel Born approximation (CCBA) analysis[18] which included inelastic effects in the incident channel gave reasonable agreement with the experimental distribution and established a means for identification of levels.

II. EXPERIMENTAL PROCEDURE AND RESULTS

A 21.1-MeV deuteron beam from the Triangle Universities Cyclo-Graaf accelerator was used to bombard a 370-μg/cm^2 self-supporting target enriched to 99.96% in ^{24}Mg. Angular distributions of scattered ^{3}He and tritons were measured simultaneously with counter telescopes in a 60-cm scattering chamber at laboratory angles from 12 to 85°. Each telescope consisted of a 1500-μm E detector and a totally depleted 50-μm ΔE detector. Pulses were amplified, summed, and stored in an on-line computer using a particle-identification program.[19]

Typical energy spectra for the ^{24}Mg$(d,t)^{23}$Mg and ^{24}Mg$(d,{}^3\mathrm{He})^{23}$Na reaction are illustrated in Fig. 1. The ^{3}He spectrum in the lower portion of the figure has been shifted by an amount comparable to the difference in the Q values for these reactions to emphasize the similarities of transitions to mirror states. These spectra illustrate that much of the strength of the (d,t) and $(d,{}^3\mathrm{He})$ reactions is concentrated in the strongly populated first excited state. It is also of interest that in each nucleus the $\frac{7}{2}^+$ and $\frac{9}{2}^+$ states near 2.0 and 2.7 MeV, respectively, were excited with moderate strength, although the shell model predicts negligible $g_{7/2}$ or $g_{9/2}$ components in the wave function for the ^{24}Mg target. The total energy resolution was 42 to 55 keV for the (d,t) reaction and 80 to 100 keV for the $(d,{}^3\mathrm{He})$ reaction. Doublets near 2.7 and 3.8 MeV in both the (d,t) and $(d,{}^3\mathrm{He})$ data were unfolded with a peak-fitting procedure. At some angles, reactions with target contaminants, ^{12}C and ^{16}O, obscured the peaks in the energy spectrum for states of ^{23}Mg. Only the ^{12}C$(d,{}^3\mathrm{He})$ reaction interfered with states of the ^{23}Na spectrum.

Angular distributions were obtained for 14 states in both ^{23}Na and ^{23}Mg. The measurements at different angles were normalized to the number of elastic counts recorded in a monitor detector, while the absolute cross sections were determined from the target thickness (measured from α-particle scattering), the solid angle subtended by the counters (0.41×10^{-3} sr) and by the beam integration. The over-all uncertainty of the absolute normalization is believed to be less than 15%.

In order to determine optical-model parameters for the reaction analysis, angular distributions were measured for deuteron and ^{3}He elastic scattering from ^{24}Mg and ^{23}Na, respectively. The deuteron-scattering experiment was essentially

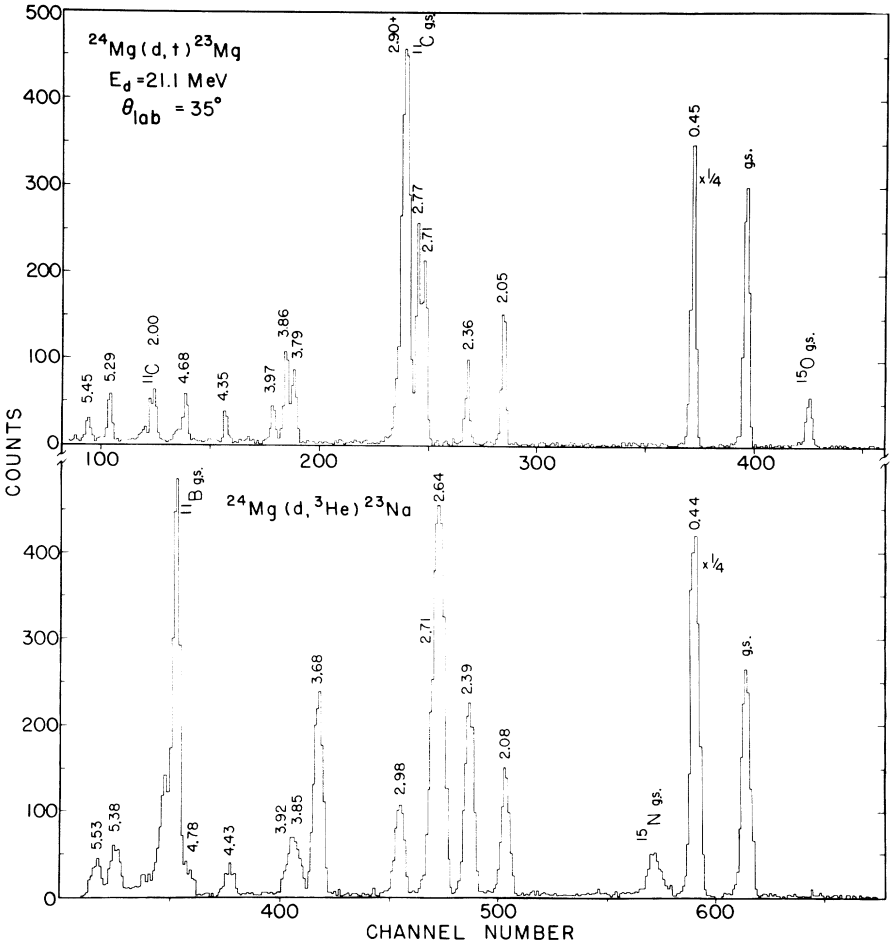

FIG. 1. Sample energy spectra for the ^{23}Mg$(d,t)^{23}$Mg and ^{24}Mg$(d,{}^3\mathrm{He})^{23}$Na reactions. The $(d,{}^3\mathrm{He})$ data have been shifted to emphasize the similarities of transitions populating states of the mirror nuclei. Peaks in the spectra are identified by excitation energies (in MeV).

the same as that for the reaction measurements except a thicker 100-μm ΔE detector was employed to improve the mass resolution. Inelastic differential cross sections for the first excited state (2_1^+) exceeded the elastic cross sections at angles >60° in the center of mass as can be seen from the angular distributions illustrated in Fig. 2. The angular distributions for inelastic scattering from the third (4_1^+) and fourth (2_2^+) excited states were also measured. The ^{3}He elastic scattering measurements at bombarding energies of 9.0 and 15.0 MeV were made with a self-supporting NaF target and counter telescopes with 17-μm ΔE detectors. The angular distributions shown in Fig. 3 were measured at two energies in order to investigate the sensitivity of the optical-model parameters to the various ^{3}He energies present in the reaction exit channel.

III. DATA ANALYSIS

A. Optical-Model Analysis

Theoretical deuteron elastic and inelastic scattering cross sections were obtained from a coupled-channel calculation with optical potentials with Woods-Saxon form factors modified by a static quadrupole deformation. As discussed by Tamura,[20] this deformation gives rise to a term in the total Hamiltonian for the scattering system which couples the states of a rotational band and introduces additional terms in the total wave function. These extra terms account for enhanced inelastic scattering from the coupled states and introduce for direct reactions additional transition amplitudes which correspond to multiple-step processes.[21] The calculations were performed using the Karlsruhe version[22] of the Tamura code JUPITOR.[23]

Starting with initial parameters given by Tjin A Djie *et al.*[24] for deuteron scattering from ^{24}Mg at 26 MeV, the parameters for scattering from the ground state and first 2^+ state were adjusted to minimize χ^2. This search determined that the deformation parameter β was 0.46, which is consistent with that obtained by other investigators.[24-26] The parameters from a detailed search that explored the Vr^n ambiguity are shown in Fig. 4. The solid lines show the results of this

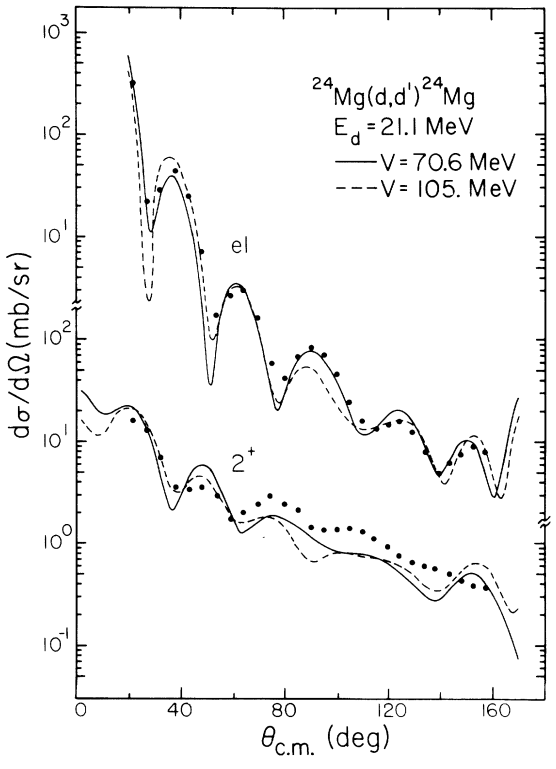

FIG. 2. ^{24}Mg(d,d')^{24}Mg angular distributions for scattering from the ground state and first 2^+ state at 1.37 MeV. The solid and broken lines represent the coupled-channel predictions obtained using parameters from the Vr^n ambiguity (see Fig. 4) with V = 70.6 and 105 MeV (see Table I), respectively.

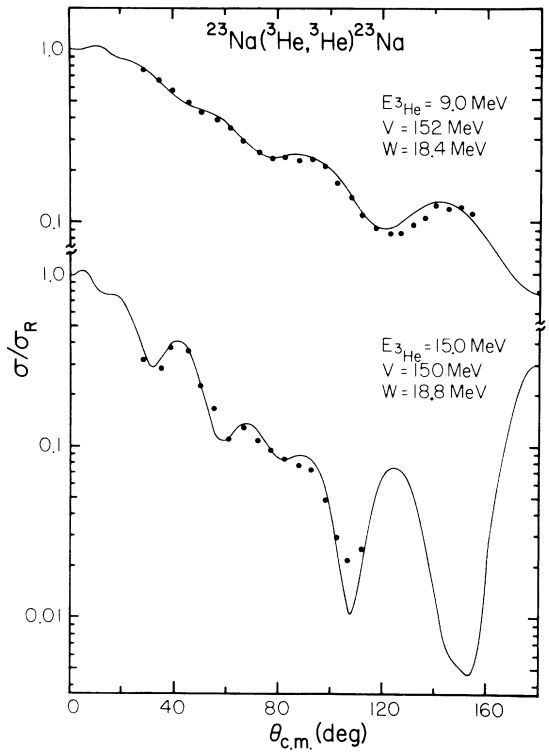

FIG. 3. ^{23}Na(^{3}He,^{3}He)^{23}Na angular distributions for elastic scattering at 9.0 and 15.0 MeV. The solid lines represent optical-model fits obtained with the geometric parameters listed in Table I and the well depths indicated with each curve.

search with the deformed potential and with a fixed deformation parameter ($\beta = 0.46$). Also shown as the broken lines are the results obtained from fitting only the elastic scattering data with the usual spherical optical model. The parameters for both potentials, which are plotted as functions of real well depth, are quite similar except for the surface absorption well depth, W_D. The lower values for the deformed potential reflect the explicit inclusion into the total wave function of the inelastic scattering from the 2_1^+ state. Since the DWBA and CCBA angular-distribution predictions were found to be sensitive to parameters from different points along the ambiguity, this figure provides a means for selection of equivalent parameters, and therefore, facilitates meaningful comparisons between the two reaction theories. Two fits for the deuteron elastic and inelastic scattering are shown in Fig. 2.

Starting with parameters determined from the predictions coupling the ground state and 2_1^+ state, the calculation was expanded to include the 4_1^+ and 2_2^+ states. Only the vibration parameter[25] γ for the 2_2^+ state and the absorption well depth W_D were adjusted to optimize the fits. With $\gamma = 20°$ and $W_D = 13$ MeV, the fits for these four states are shown in Fig. 5. Both the shapes and magnitudes of the predicted distributions for these additional levels were in good agreement with the data, although the quality of the resulting fit for the elastic scattering declined somewhat.

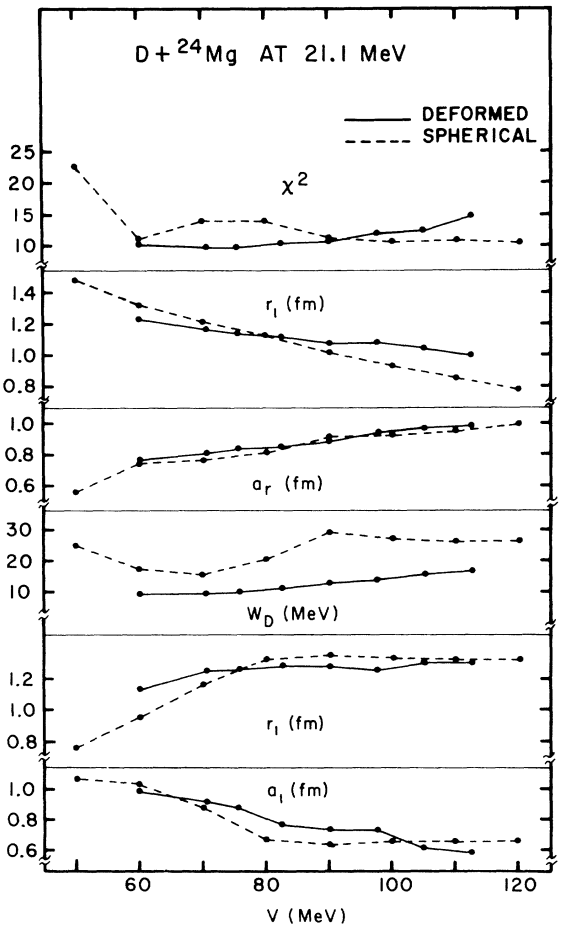

FIG. 4. Optical-model parameters for 21.1-MeV deuteron scattering from ^{24}Mg. The optical-model parameters for deformed (spherical) potentials, which yield a minimum χ^2 with fixed deformation $\beta = 0.46$ (0.0), are indicated by the solid (broken) line for various real well depths V. These parameters constitute what is termed the Vr^n continuous ambiguity (see Fig. 6).

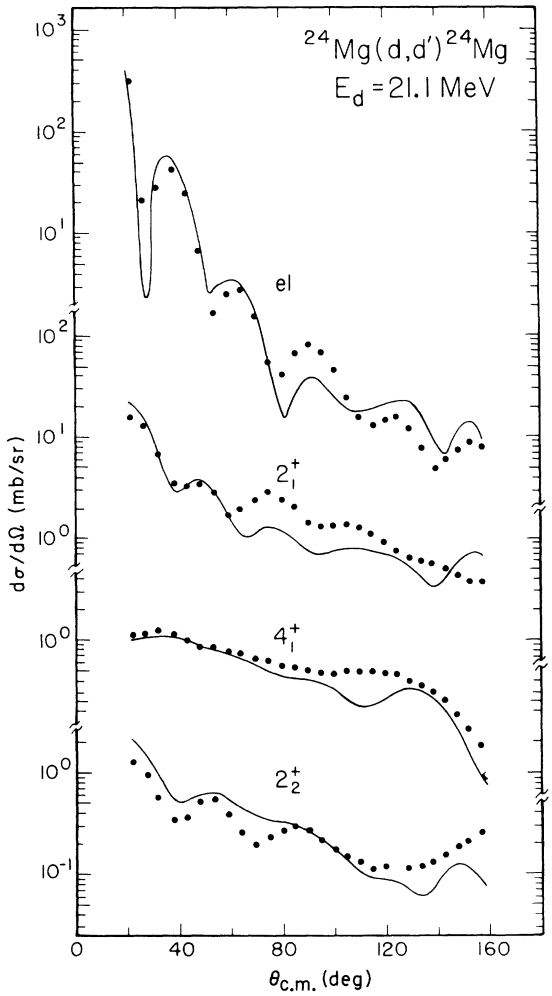

FIG. 5. ^{24}Mg$(d,d')^{24}$Mg angular distributions for scattering from the ground state and 2_1^+, 4_1^+, and 2_2^+ excited states. The solid lines represent coupled-channel predictions for these four states with parameters $\gamma = 20°$, $W_D = 13.0$ MeV, and the others from the deformed potential listed in Table I.

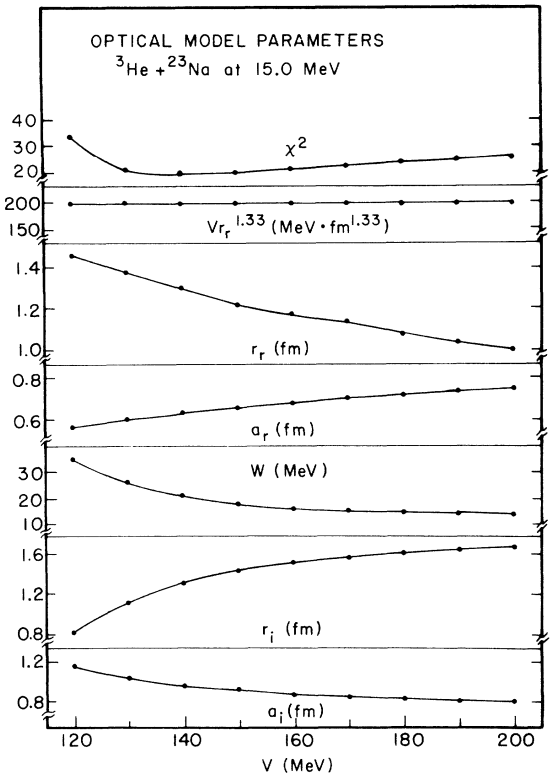

FIG. 6. Optical-model parameters for 15.0-MeV ^{3}He scattering from ^{23}Na. The optical-model parameters for spherical potentials which yield a minimum χ^2 are plotted for various real well depths V. As may be seen from the second curve from the top, the product $Vr^{1.33}$ remains constant over the range of V shown.

Optical-model parameters for the ^{3}He scattering in the exit channel were determined from a search analogous to that performed for the deuterons scattering except only the usual spherical potentials were considered. A more complicated coupled-channel search was considered unnecessary, since the inelastic scattering at backward angles was observed to be a factor of 10 weaker than the elastic scattering. The curve shown in Fig. 3 for the 15.0-MeV data represents the fit for minimum χ^2 with a real well depth of 150 MeV. With the same geometric parameters for the potentials, the well depths were adjusted to give best fit to the 9.0-MeV data which is also shown in Fig. 3. The well depths obtained in this calculation differed only slightly from those for the 15.0-MeV data indicating the energy dependence of the optical-model parameters may not be very sensitive over this energy range. Fitting only the 15.0-MeV ^{3}He scattering data, a search over the Vr^n ambiguity yielded the results displayed in Fig. 6.

B. CCBA and DWBA Analysis

In order to investigate the importance of two-step processes, both CCBA and DWBA cross sections were computed for comparisons with each other and with the data. Since the DWBA is a special case of the CCBA, all calculations were performed with the Tamura computer code MARS[27] which employes the CCBA formalism as discussed by Penny and Satchler.[21] Optical-model parameters for the entrance and exit reaction channels were selected from the continuous ambiguities shown in Figs. 4 and 6. By varying combinations of parameters associated with the only two free parameters, the real well depths, the CCBA fits were found to be optimized for the values listed in Table I. The triton parameters were chosen to be identical with the ^{3}He parameters; only the Coulomb term was different for the $Z = 1$ and $Z = 2$ particles.

The form factors for the analysis were computed assuming a spherical-well potential with Woods-Saxon shape with radius $r_0 = 1.25\ A^{1/3}$ fm, diffuseness $a = 0.65$ fm, spin-orbit strength $\lambda = 25.0$, and a well depth V_0 adjusted to give the correct separation energy for the bound particle. Proper separation energies for inelastic processes should be decreased by the inelastic excitation energy from those required for the competing direct transitions. Since the separation energies for the direct processes were large, this small adjustment was neglected. Similarly, the use of a spherical potential for the ground

TABLE I. Optical-model parameters.

Channel	E_{lab} (MeV)	β [a]	V (MeV)	r_0 (fm)	a_0 (fm)	W (MeV)	W_D (MeV)	r_i (fm)	a_i (fm)	r_C (fm)
^{24}Mg + d	21.1	0.46	105	1.041	0.963	···	15.0	1.31	0.629	1.30
^{24}Mg + d	21.1	0.00	100	0.928	0.918	···	26.7	1.32	0.664	1.30
^{23}Na + ^{3}He [b]	15.0	0.00	150	1.244	0.650	18.8	···	1.43	0.921	1.40

[a] The deformation parameter β is denoted as 0.0 for channels where inelastic scattering was neglected.
[b] Optical-model parameters for ^{23}Na + ^{3}He were also adopted for the ^{23}Mg + t channel.

TABLE II. Values of the Nilsson coefficients $C_{j\Omega}$ as obtained from deformed-well calculations (see Ref. 29).

$\Omega^{\pi}[Nn_z\Lambda]$ j	$\frac{1}{2}^+[220]$	$\frac{3}{2}^+[211]$	$\frac{1}{2}^+[211]$	$\frac{5}{2}^+[202]$	$\frac{1}{2}^+[200]$	$\frac{1}{2}^-[101]$ [a]
$\frac{1}{2}$	−0.452	0.0	−0.548	0.0	−0.705	0.938
$\frac{3}{2}$	−0.180	−0.193	−0.711	0.0	0.665	0.347
$\frac{5}{2}$	0.864	0.970	−0.425	0.993	−0.222	0.0
$\frac{7}{2}$	−0.028	−0.044	−0.086	−0.042	0.099	0.0
$\frac{9}{2}$	0.130	0.138	−0.080	0.115	−0.048	0.0

[a] Calculation with simple Nilsson model with anisotropic harmonic-oscillator potential ($\eta=4.0$, $\kappa=0.10$, $\mu=0.16$).

state was an additional approximation affecting the form factor which, according to Rost,[28] also introduced small deviations in the theoretical cross sections relative to calculations employing a more realistic deformed potential.

Since the direct and indirect contributions to the cross section add coherently, the CCBA calculation is not well suited for the direct extraction of spectroscopic amplitudes for the various contributions. However, through comparisons with experimental angular distributions, CCBA predictions provide an excellent means for evaluating the validity of amplitudes defined by various models. Initially all of the amplitudes were estimated from the collective model (including band mixing) with Nilsson coefficients $C_{j\Omega}$ obtained from a coupled-channel calculation for bound states[29] (see Table II). The band-head energies E_0^{Ω} and inverse moments of inertia A required for the calculation were selected to give a best fit to the energy spectrum of ^{23}Mg. These parameters and the occupation number V_{Ω}^2 are listed in Table III for each band included in the calculation. The derived spectroscopic amplitudes A_j for direct and indirect transitions from the 2_1^+ and 4_1^+ members of the ^{24}Mg ground-state rotational band are indicated in Table IV. Except for the $\frac{11}{2}^+$ final states, the CCBA calculations reported in this study do not include indirect transitions through the 4_1^+ and 2_2^+ state of ^{24}Mg. Recently, all of the CCBA predictions for states of positive parity have been recalculated using the amplitudes obtained from a truncated shell-model calculation by Wildenthal.[30] Table V lists these shell-model amplitudes.

TABLE III. Parameters used in bandmixing calculations.

$\Omega^{\pi}[Nn_z\Lambda]$	$A=\hbar^2/2\mathcal{I}$ (MeV)	E_0^{Ω} (MeV)	V_{Ω}^2 [a]
$\frac{1}{2}^+[220]$	0.20	4.23	1.00
$\frac{3}{2}^+[211]$	0.21	0.0	0.70
$\frac{1}{2}^+[211]$	0.19	2.28	0.20
$\frac{5}{2}^+[202]$	0.18	5.50 [b]	0.08
$\frac{1}{2}^+[200]$	0.17	6.17 [b]	0.02
$\frac{1}{2}^-[101]$	0.19	2.77	1.00

[a] Adapted from Ref. 29.
[b] Adjusted to reproduce the band-head energies of ^{23}Na.

The angular distributions measured for the ^{24}Mg$(d,{}^3\text{He})^{23}$Na and ^{24}Mg$(d,t)^{23}$Mg reactions are shown in Figs. 7–11. Selected angular distributions are reproduced in Fig. 7 for comparisons with both the CCBA and DWBA predictions. The DWBA calculations were made with deuteron optical-model parameters for spherical potentials selected with nearly the same real well depth as those used for the CCBA calculations (see Fig. 4 and Table I). Identical ^{3}He parameters for the exit channel and identical spectroscopic amplitudes and form factors for the direct transitions were used in both the DWBA and CCBA calculations. Only collective-model spectroscopic amplitudes were employed in the theoretical distributions shown in Fig. 7.

In Figs. 8–11, only the CCBA calculations are shown and the results for collective-model and shell-model amplitudes are represented by the solid and broken curves, respectively. The angular distributions of states identified with each rotational band are grouped together, and the mirror levels are shown beside one another. The computer code evaluated absolute cross sections from the spectroscopic amplitudes and normalization constants D_0^2 defined within the program as 2.99 and 3.37 for the $(d,{}^3\text{He})$ and (d,t) reactions, respectively. The additional factors N required to normalize the predictions to the data are shown for each curve, and deviations from unity reflect failures of the CCBA theory and/or nuclear model.

TABLE IV. Pickup spectroscopic amplitudes A_j determined from the collective model including band mixing.

Nilsson orbit	Energy in ^{23}Na (MeV)	Spin and parity J^π	A_j for $0^+ \to J^\pi$	A_j for $2^+ \to J^\pi$ $j=\frac{1}{2}$	$\frac{3}{2}$	$\frac{5}{2}$	A_j for $4^+ \to J^\pi$ $\frac{1}{2}$	$\frac{3}{2}$	$\frac{5}{2}$
$\frac{3}{2}^+[211]$	0.00	$\frac{3}{2}^+$	−0.218	0.025	−0.105	0.704	0.000	0.000	0.132
	0.44	$\frac{5}{2}^+$	1.510	−0.083	0.153	−0.279	0.000	0.046	−0.370
	2.08	$\frac{7}{2}^+$	−0.053	0.000	−0.103	−0.693	0.043	−0.122	0.511
	2.71	$\frac{9}{2}^+$	0.239	0.000	0.000	1.018	−0.130	0.133	−0.135
	5.53	$\frac{11}{2}^+$	0.000	0.000	0.000	0.000	0.000	−0.079	−0.703
$\frac{1}{2}^+[211]$	2.39	$\frac{1}{2}^+$	−0.322	0.000	−0.190	−0.149	0.000	0.000	0.000
	2.98	$\frac{3}{2}^+$	−0.497	0.231	0.207	0.010	0.000	0.000	0.090
	3.92	$\frac{5}{2}^+$	−0.080	−0.251	0.146	0.152	0.000	−0.199	−0.199
	4.78	$\frac{7}{2}^+$	−0.068	0.000	−0.365	−0.062	0.238	0.182	0.013
$\frac{1}{2}^+[220]$	4.43	$\frac{1}{2}^+$	−0.657	0.000	−0.124	0.539	0.000	0.000	0.000
	5.38	$\frac{5}{2}^+$	0.707	−0.481	0.049	−0.574	0.000	−0.153	0.405
$\frac{1}{2}^-[101]$	2.64	$\frac{1}{2}^-$	1.326	0.000	0.220	0.000	0.000	0.000	0.000
	3.68	$\frac{3}{2}^-$	0.491	−0.839	−0.220	0.000	0.000	0.000	0.000
	3.85	$\frac{5}{2}^-$	0.000	1.055	0.021	0.000	0.000	0.263	0.000

IV. DISCUSSION

A. DWBA and CCBA Predictions and Comparisons

In a single-step direct reaction the angular distributions characterized by the same orbital angular momentum (l) transfer are usually similar in shape unless the energies of the scattered particles differ greatly. In this experiment the data show rather pronounced differences for $l=2$ transitions from neighboring states which are members of different rotational bands. Angular distributions shown in Fig. 7 for the $\frac{3}{2}^+$ and $\frac{5}{2}^+$ members of the ground-state rotational band and

TABLE V. Pickup spectroscopic amplitudes A_j determined from the shell model (see Ref. 30). The excitation energies are arranged to correspond to the order in Table IV.

Energy in ^{23}Na (MeV)	Spin and parity J^π	A_j for $0^+ \to J^\pi$	A_j for $2^+ \to J^\pi$ $j=\frac{1}{2}$	$\frac{3}{2}$	$\frac{5}{2}$	A_j for $4^+ \to J^\pi$ $\frac{5}{2}$
0.00	$\frac{3}{2}^+$	0.278	−0.095		−0.962	
0.44	$\frac{5}{2}^+$	1.652	0.245		0.544	
2.08	$\frac{7}{2}^+$	0.000	0.000	0.164	−0.581	
2.71	$\frac{9}{2}^+$	0.000	0.000	0.000	−0.985	−0.490
5.53	$\frac{11}{2}^+$	0.000	0.000	0.000	0.000	−0.454
2.39	$\frac{1}{2}^+$	0.473	0.000	0.190	0.249	
2.98	$\frac{3}{2}^+$	0.365	−0.260		−0.039	
3.92	$\frac{5}{2}^+$	−0.164	−0.299		−0.187	
4.78	$\frac{7}{2}^+$	0.000	0.000	0.190		
4.43	$\frac{1}{2}^+$	0.177	0.000	−0.023	0.326	
5.38	$\frac{5}{2}^+$	−0.436	−0.114		−0.242	

the $\frac{3}{2}^+$ (2.98-MeV) state of the lowest $\frac{1}{2}^+$ band illustrate typical variations for the $(d, {}^3\mathrm{He})$ reaction. As expected, the DWBA predictions for these levels (broken lines) have essentially the same shape. While the DWBA calculation for the $\frac{5}{2}^+$ state is rather good, the prediction for the $\frac{3}{2}^+$ (2.98-MeV) state in the $\frac{1}{2}^+$ band does not describe the shape of any portion of the distribution. The fit for the ground-state transition is reasonable at forward angles, but it fails to predict the behavior at back angles. Neither the shape nor the magnitude ($N = 360$) of the theoretical DWBA cross section agree with angular distribution for the "j-forbidden" $\frac{7}{2}^+$ state.

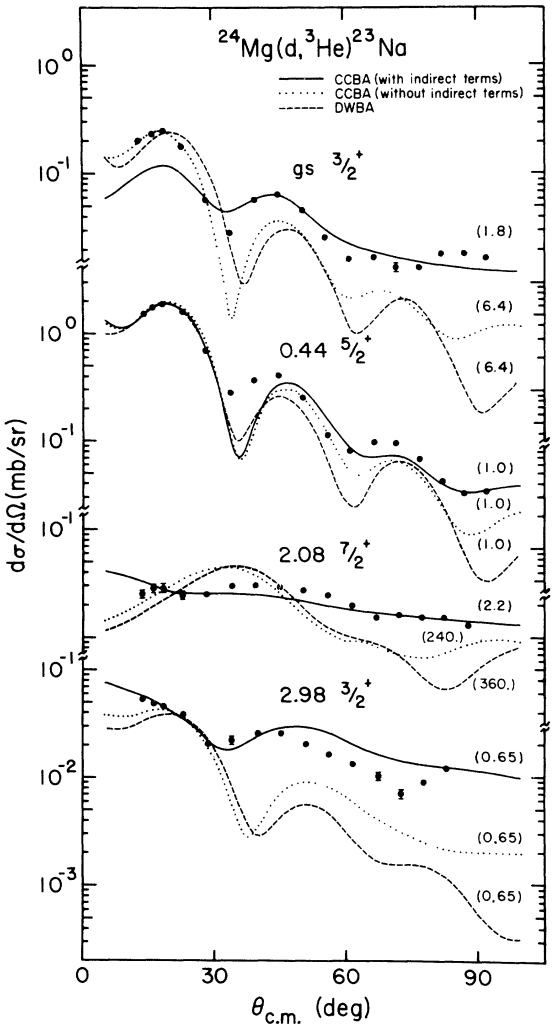

FIG. 7. Comparisons of DWBA and CCBA calculations. The solid curves are the results of the full CCBA calculation which included both direct and indirect terms populating the final state. Also shown are the results of the CCBA calculation where only the direct term was included (dotted line). The DWBA calculations (broken lines) employed a spherical optical-model potential similar to the deformed potential used in the CCBA calculation. The number indicated with each curve is the factor required to normalize the prediction to the data. This factor should be near unity (see text).

CCBA predictions were computed for these same states where indirect transitions through the first 2^+ state of ^{24}Mg were first excluded (dotted lines) and then included (full lines). As seen in Fig. 7, the predictions of this first calculation, analogous to DWBA but employing optical-model wave functions obtained from a coupled-channel calculation, did not describe the data, but, in fact nearly reproduced the DWBA predictions. However, by including the two-step processes for the full CCBA calculation, reasonable agreement was obtained for all levels. It should be emphasized that this agreement must be attributed to the inclusion of inelastic processes rather than a fortuitous choice of optical-model parameters, since identical CCBA calculation without these indirect terms produced essentially the same results as the usual DWBA.

Several features of the fits shown in Fig. 7 merit further comment. The three predictions for the 0.44-MeV level produced equally good fits to the data. As seen in Table IV, this $\frac{5}{2}^+$ level has a very large direct term and only weak indirect contributions. Hence the reaction is essentially direct, and the good DWBA fit merely reflects the validity of that approximation for this transition. On the other hand, the calculated angular distributions for the 2.98-MeV level changed significantly upon the introduction of rather large indirect components. The indirect terms tend to make the predictions more isotropic, particularly at the backward angles when the direct contributions are weak. This same trend is seen in the spectacular CCBA fit which explains both the shape and magnitude ($N \simeq 2$) for the $\frac{7}{2}^+$ level at 2.08 MeV.

The calculated ground-state angular distributions also changed significantly in shape and amplitude, but the change was less encouraging since the forward stripping peak was reduced with respect to the second maximum. To investigate the effect of different relative amounts of direct and indirect scattering upon the shapes of these cross sections, the spectroscopic amplitude of the direct term was increased by a factor of 3 while holding the inelastic terms constant. The results, represented by the solid curves in Fig. 12(a), give a considerably improved description of the data for transitions to both ^{23}Na and ^{23}Mg. This improvement suggests that the wave function used in the calculation of the spectroscopic amplitude is probably incorrect. Such a conclusion is consistent with the fact that other pickup re-

actions studied at higher energies, where the effects of two-step processes are diminished, have indicated that the experimental spectroscopic factors for the ground-state transition are greater than either collective- or shell-model predictions by a factor of 5–10 (see columns 6–8, 10, 11 of Table VI).

Additional calculations were performed to determine the influence of various spectroscopic amplitudes contributing to the inelastic processes. If DWBA were to serve as a guide, one would expect little difference between transfers with the same orbital angular momentum even though the total angular momentum transfers $j = (l + s)$ were different. However, as seen in Fig. 12(b), the predictions are quite sensitive to the j of the nucleon transferred in the inelastic process. The solid and dotted curves show the results for pure $d_{3/2}$ and $d_{5/2}$ transfers in the two-step processes, respectively. The broken line is the distribution obtained using a mixture of both with amplitudes predicted by the collective model. In each case the form factor may be expressed as the sum $\alpha d_{3/2} + \beta d_{5/2}$, where $\alpha^2 + \beta^2 = (0.24)^2$, so that the total $l = 2$ indirect amplitude is conserved. Indirect transfers with only the $d_{5/2}$ component give the best fit to the data. Similar calculations for other states exhibited this j dependence, although the changes were not so pronounced. Clearly, some of the discrepancies between the CCBA predictions and experimental angular distributions may be explained by adjustments of the spectroscopic amplitudes.

This analysis, as was previously noted, has made certain simplifying assumptions in order to treat a rather complex physical situation in a simple but meaningful way. There has been no systematic attempt to include inelastic contributions through the 4_1^+ or 2_2^+ states of ^{24}Mg. One notable exception is the cross-section prediction for the $\frac{11}{2}^+$ state observed in each ground-state rotational band which must proceed through the 4_1^+ state. For other states the omission of this term is unlikely to be very significant, since calculations for the $\frac{7}{2}^+$ state of the ground-state rotational bands, which included a relatively large $J = \frac{5}{2}$ component through the 4_1^+ state, showed only minor differences in shape and magnitude. A decrease in the separation energy by the inelastic excitation energy was neglected for the description of two-step form factors. Sample calculations for several states indicated that this approximation had little

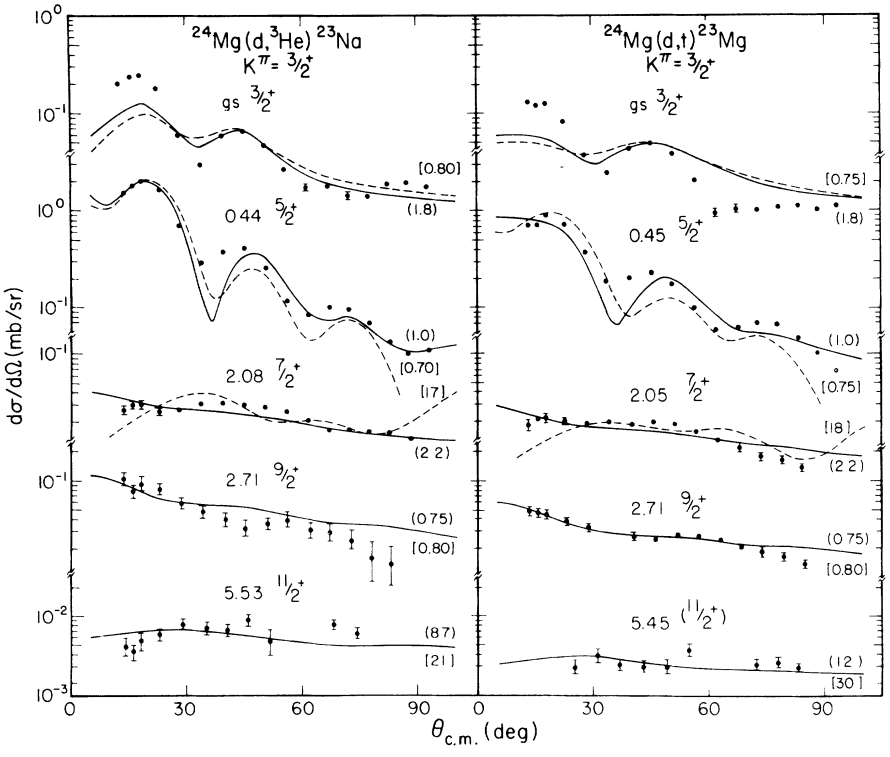

FIG. 8. ^{24}Mg(d, ^{3}He)^{23}Na and ^{24}Mg(d,t)^{23}Mg angular distributions identified with transitions to the ground-state $K^\pi = \frac{3}{2}^+$ band of the collective model. The CCBA predictions using collective-model (shell-model) spectroscopic amplitudes are represented by the solid (broken) curves with normalization factors given in curved (square) brackets.

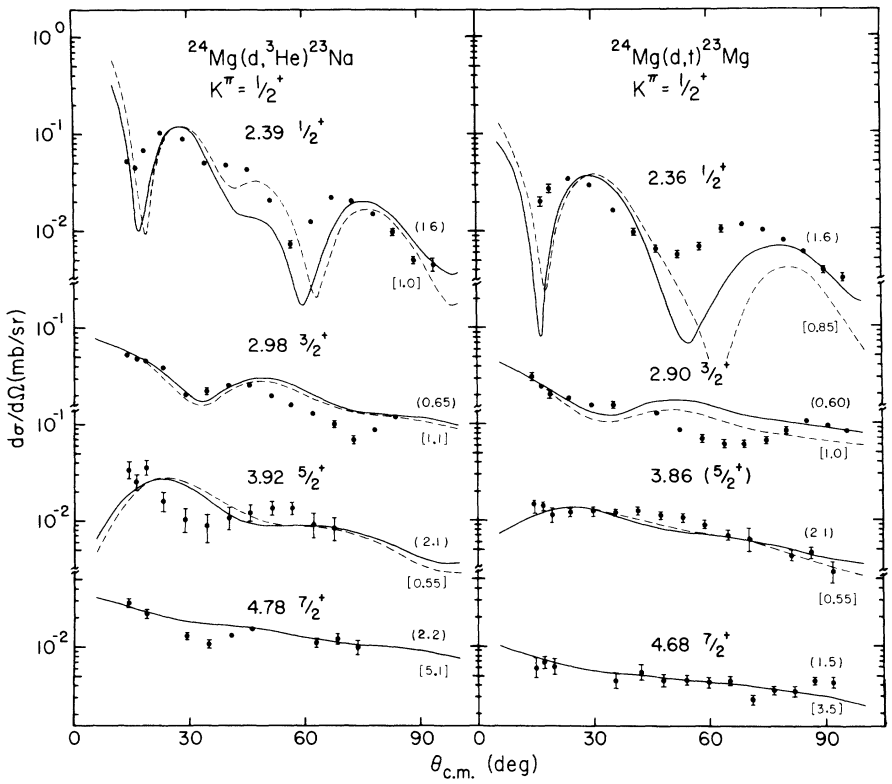

FIG. 9. ^{24}Mg(d, ^{3}He)^{23}Na and ^{24}Mg(d,t)^{23}Mg angular distributions identified with transitions to the lowest $K^{\pi}=\frac{1}{2}^{+}$ band. See Fig. 8 for additional comment.

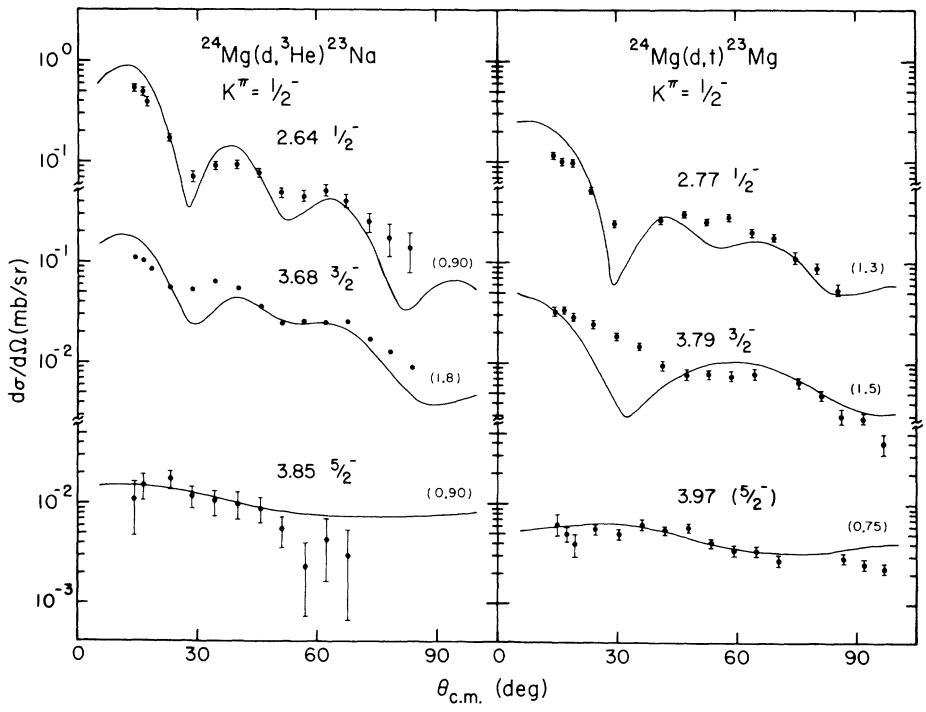

FIG. 10. ^{24}Mg(d, ^{3}He)^{23}Na and ^{24}Mg(d,t)^{23}Mg angular distributions identified with transitions to the lowest $K^{\pi}=\frac{1}{2}^{-}$ band. See Fig. 8 for additional comment.

effect upon the shape of the CCBA predictions and changed the magnitude no more than 20%.

B. Structure of ^{23}Mg and ^{23}Na

The CCBA cross-section calculations generally agreed well with the experimental data shown in Figs. 8–11. The small differences in shape between CCBA predictions employing spectroscopic amplitudes determined by the collective model and shell model were not considered significant, since similar changes were also produced with 5–10% variations in the optical-model parameters. Only a few of the predictions required more than a factor of 2 in order to normalize the calculated curves to the experimental data. It is of interest that the normalization factors N which are given for each curve have nearly equal values for known mirror levels populated with the $(d, {}^3\mathrm{He})$ and (d, t) reactions. This equality indicated that the charge asymmetry of the two reactions was correctly described by the CCBA and form-factor calculations, and therefore provides a means of discrimination between states with angular distributions similar in shape but different in magnitude. The CCBA calculations also discriminated between the two $\frac{7}{2}^+$ shell-model states[17] predicted to lie between 4 and 5 MeV; the upper $\frac{7}{2}_3$ was identified with the 4.78 (4.68)-MeV state in ^{23}Na(^{23}Mg), since the spectroscopic amplitudes for the $\frac{7}{2}_2$ state were too small to give agreement with experiment.

On the basis of the CCBA fits it was possible to obtain new J^π assignments for seven states in ^{23}Mg through identification with the mirror

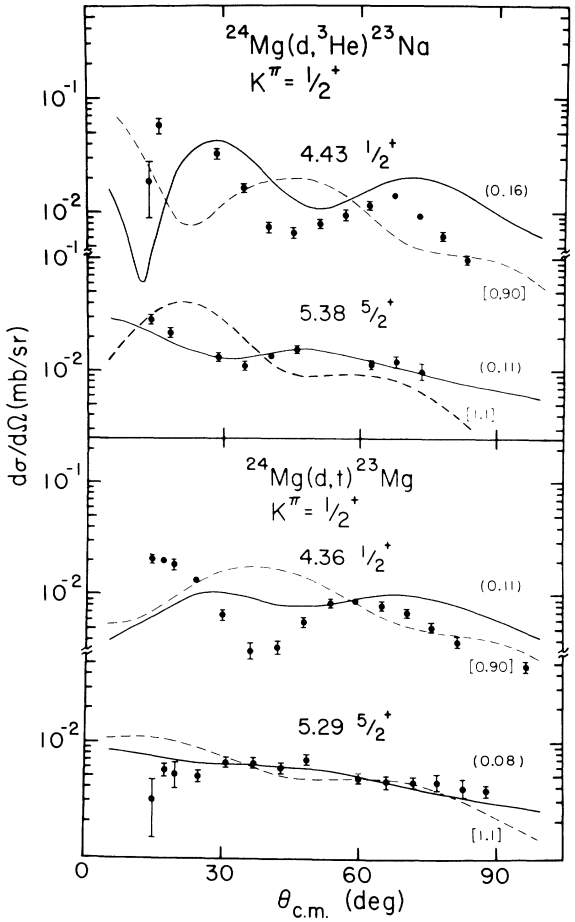

FIG. 11. ^{24}Mg$(d, {}^3\mathrm{He})^{23}$Na and ^{24}Mg$(d,t)^{23}$Mg angular distributions identified with transitions to the second $K^\pi = \frac{1}{2}^+$ band. See Fig. 8 for additional comment.

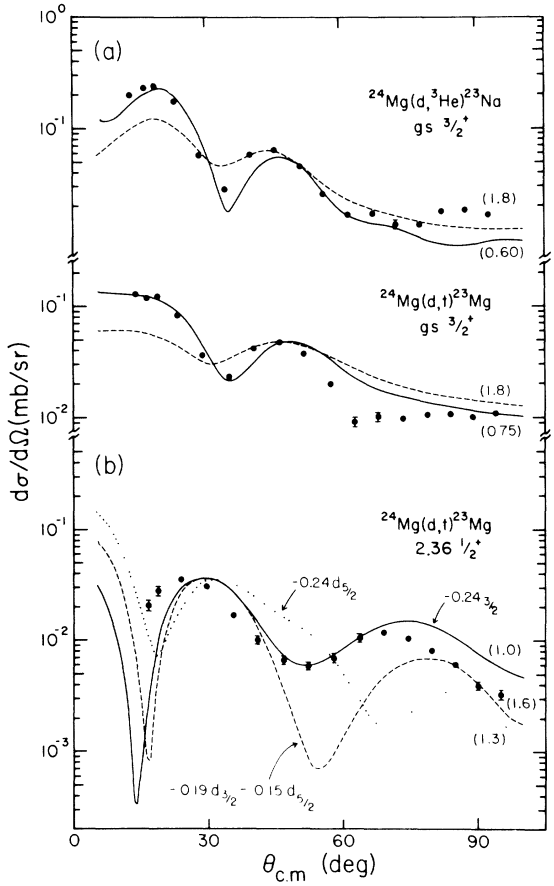

FIG. 12. Comparisons of CCBA calculations for variations in the spectroscopic amplitudes. Part (a) shows that the prediction for the ground-state transitions may be improved by increasing the spectroscopic amplitude for the direct term by a factor of 3 (solid lines). The unmodified fits of Fig. 8 are reproduced here for comparisons (broken lines). Part (b) shows the sensitivity of a $J^\pi = \frac{1}{2}^+$ angular distribution to the amplitudes assumed for the indirect coupling terms. For each case illustrated the amplitudes satisfy $\alpha d_{3/2}{}^+ \; \beta d_{5/2}$ where $\alpha^2 + \beta^2 = \text{constant}$.

states in ^{23}Na. To establish a pair of states as analogs, it was necessary that the CCBA predictions give reasonably good *fits* and similar *normalizations* for both angular distributions with identical coupling schemes and spectroscopic amplitudes. In this way J^π assignments of $\frac{9}{2}^+$, $\frac{3}{2}^+$, $(\frac{7}{2}^+)$, and $(\frac{5}{2}^+)$ were established for levels at 2.71, 2.90, 4.68, and 5.29 MeV with identification of the mirror states in ^{23}Na at 2.71, 2.98, 4.78, and 5.38 MeV, respectively. The determination of these mirror states was considerably simplified as there were no angular distributions with similar shapes and magnitudes lying near in excitation energy. The proximity of states at 3.86 and 3.97 MeV in ^{23}Mg and similarity of the structure of the angular distributions hindered identification of these levels. Fortunately, the magnitudes differed significantly, indicating that the 3.86- and 3.97-MeV levels were the mirror states of the $\frac{5}{2}^+$, and $\frac{5}{2}^-$ levels in ^{23}Na at 3.92 and 3.85 MeV, respectively. If these assignments were reversed as in previous work,[9] the normalization factors N would not agree as they should for mirror states. The present parity assignments are consistent with the Coulomb energy systematics for the *sd* shell as noted by Everling[31] and are in excellent agreement with a Coulomb energy calculation of de Meijer, van Royen, and Brussaard[32] which predicts the mirror for the 3.92-MeV $\frac{5}{2}^+$ state of ^{23}Na to lie at 3.88 MeV in ^{23}Mg.

The recent identification[15] of an $\frac{11}{2}^+$ state in ^{23}Na prompted our CCBA calculations which included indirect transitions through the 4_1^+ state of ^{24}Mg. These calculations give essentially the correct shape for the distributions but not the proper magnitudes. The $\frac{11}{2}^+$ assignment in ^{23}Mg is regarded as tentative. Figure 13 displays the energy-level diagram which summarizes the J^π assignments from this work and from previous studies. The energy levels from the collective-model calculations are also compared with experiment. A similar comparison for the shell-model calculation is given in Ref. 17.

Experimental spectroscopic factors for $l=0$, 1, and 2 transitions were calculated to facilitate comparisons with other work. Since these values could not be obtained from the usual normalization of DWBA fits, the spectroscopic factors were calculated from an *ad hoc* approach as the product of the square of the theoretical spectroscopic amplitude for the direct transition times the normalization factor N given for each CCBA prediction. In cases where the theoretical cross sections were dominated by direct contributions, this number was equivalent to the usual spectroscopic factor. Values from CCBA calculations with shell-model

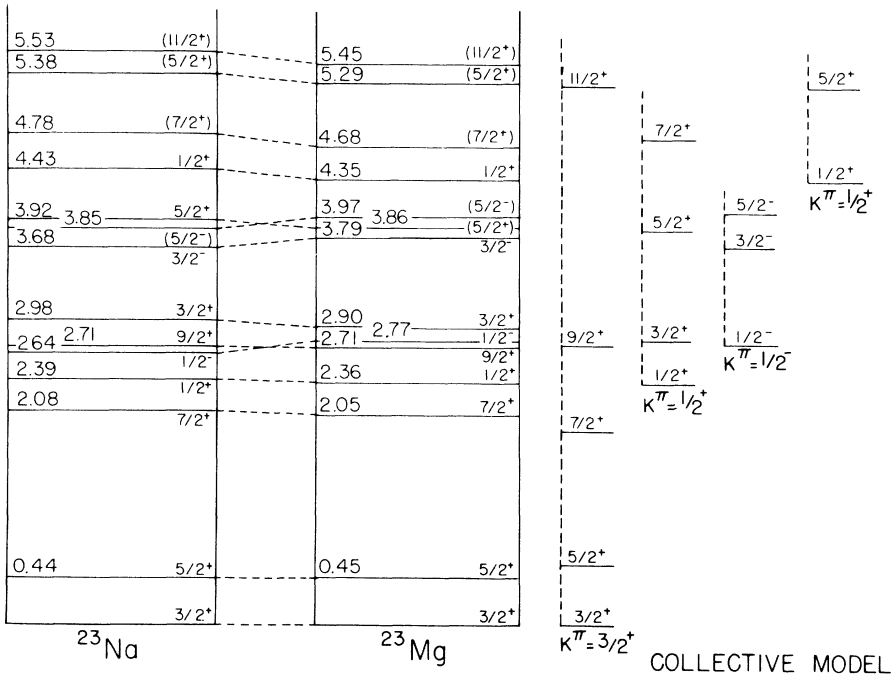

FIG. 13. ^{23}Na and ^{23}Mg energy-level diagrams and collective-model predictions. The J^π assignments for ^{23}Na were taken from Refs. 7 and 15, and those for ^{23}Mg were obtained from the present study and Refs. 9 and 14. The energy spectrum predicted by the collective-model calculation with parameters from Tables II and III is also illustrated.

and collective-model spectroscopic amplitudes were averaged. As seen in Table VI, the spectroscopic factors obtained by this procedure are in general agreement with those determined from different reactions measured at higher energies and analyzed with DWBA.

The application of the sum rules with the experimental spectroscopic factors taken from columns 4 and 5 of Table VI shows that for positive-parity states, $\sum C^2S = 3.0$ for ^{23}Na and ^{23}Mg where the shell-model limit is $\sum C^2S = 4$. The concentration of the spectroscopic strength in the ground-state rotational band, $\sum C^2S = 2.4$, exceeds the limit of 2 for a single Nilsson orbit thereby implying that band mixing is necessary in the collective model for ^{23}Na and ^{23}Mg. The shell-model calculation correctly predicts this large strength. The negative-parity strength, $\sum C^2S = 2.0$; (2.7), for the $\frac{1}{2}^-$ [101] band in ^{23}Na(^{23}Mg) indicates that most of the total p-shell strength (limit $\sum C^2S = 6$) is associated with higher unobserved states.

In contrast with the over-all success of the present treatment, the predictions for the $\frac{1}{2}^+$[220] rotational band (Fig. 10) with states above 4 MeV gave poor agreement with experiment. With the exception of the 4.36-MeV level in ^{23}Mg, the structure of the angular distributions calculated with collective spectroscopic amplitudes were fairly well described, but the magnitudes were a factor of ~10 too large. On the other hand, cross-section predictions with shell-model amplitudes gave reasonable agreement with the magnitudes but not the shape of the distributions.

The CCBA calculations with shell-model amplitudes for the $\frac{7}{2}^+$ members of the ground-state rotational band also failed to give agreement with the data or with the collective-model prediction. Inspection of Tables IV and V shows that the $j = \frac{3}{2}$ and $\frac{5}{2}$ amplitudes have a relative sign change for the shell model, whereas those of the collective model do not. Although the magnitudes of these amplitudes do not differ greatly, the CCBA pre-

TABLE VI. Spectroscopic results of the ^{24}Mg(d, ^{3}He)^{23}Na and ^{24}Mg(d, t)^{23}Mg reactions and predictions of the nuclear models.

Energy ^{23}Na (MeV)	Energy ^{23}Mg (MeV)	Spin and parity J^π	C^2S (d, ^{3}He) (21 MeV) [a]	(d, t) (21 MeV) [a]	(d, ^{3}He) (52 MeV) [b]	(d, ^{3}He) (82 MeV) [c]	(p, d) (34 MeV) [d]	Collective model [e] K^π	C^2S	Shell model [f] C^2S
0.00	0.00	$\frac{3}{2}^+$	0.26 [g]	0.33 [g]	0.24	0.47	0.36	$\frac{3}{2}^+$	0.052	0.078
0.44	0.45	$\frac{5}{2}^+$	2.1	2.2	3.78	2.90	2.83	$\frac{3}{2}^+$	2.28	2.73
2.08	2.05	$\frac{7}{2}^+$						$\frac{3}{2}^+$	0.003	
2.39	2.36	$\frac{1}{2}^+$	0.19	0.18	0.30	0.25	0.10	$\frac{1}{2}^+$	0.10	0.22
2.64	2.77	$\frac{1}{2}^-$	1.6	2.3	2.64	2.10	1.70	$\frac{1}{2}^-$	1.76	
2.71	2.71	$\frac{9}{2}^+$						$\frac{3}{2}^+$	0.057	
2.98	2.90	$\frac{3}{2}^+$	0.15	0.14	0.17	0.34		$\frac{1}{2}^+$	0.25	0.13
3.68	3.79	$\frac{3}{2}^-$	0.43	0.36	0.93	0.85	0.85	$\frac{1}{2}^-$	0.24	
3.85	3.97	$(\frac{5}{2}^-)$						$\frac{1}{2}^-$	0.00	
3.92	3.86	$\frac{5}{2}^+$	0.014	0.014	0.02			$\frac{1}{2}^+$	0.006	0.027
4.43	4.35	$\frac{1}{2}^+$	0.064	0.053	0.12	0.08	0.05	$\frac{1}{2}^+$	0.43	0.032
4.78	4.68	$(\frac{7}{2}^+)$						$\frac{1}{2}^+$	0.005	
5.38	5.29	$(\frac{5}{2}^+)$	0.21 [h]	0.21 [h]	0.49	0.42	0.27	$\frac{1}{2}^+$	0.50	0.19
5.53	5.45	$(\frac{11}{2}^+)$						$\frac{3}{2}^+$	0.00	

[a] Present study. Here $C^2S = \overline{N}A_j^2$ where N is the additional normalization factor indicated for each curve in Figs. 8–11. The A_j are the direct transition spectroscopic amplitudes listed in Tables IV and V.
[b] Reference 12.
[c] Reference 11.
[d] Reference 2.
[e] $C^2S = A_j^2$ of Table IV.
[f] $C^2S = A_j^2$ of Table V.
[g] Here $A_j = 3A_j$ of Table IV. N is taken from Fig. 12(a).
[h] Values only from shell-model calculations.

dictions exhibited a strong sensitivity to the phase and provided a test of the wave function not available in the usual DWBA.

The general consistency of the spectroscopic factors listed in Table VI suggested a brief investigation of the CCBA analysis for reactions induced at higher bombarding energies. Calculations were performed to describe several angular distributions from the ^{24}Mg$(d, ^3$He$)^{23}$Na reaction measured by Kramer, Mairle, and Kaschl[12] at 52 MeV. Employing slightly modified optical-model parameters from those given by Kramer, Mairle, and Kaschl and the deformation parameter obtained from this study, the CCBA predictions were found to be essentially identical whether or not the indirect terms were included. Furthermore, since they agreed with the DWBA fit obtained by Kramer, Mairle, and Kaschl, the CCBA analysis appears equivalent to the usual DWBA treatment for reaction studies at higher bombarding energies.

V. CONCLUSION

Our calculations have shown that the CCBA can successfully describe the multiple-step processes present in the single-nucleon pickup reactions of this study. These processes were found not only to dominate the transitions to the "j-forbidden" states, but to have significant effects upon the angular distributions for allowed transitions with $l \leq 2$ as well. Calculations with spectroscopic amplitudes from both the collective model and shell model indicated that the CCBA predictions exhibit a sensitivity to many terms of the nuclear wave functions not considered by the usual DWBA. Of course this sensitivity is strongly enhanced if the angular distributions are measured at bombarding energies where the inelastic scattering is large relative to elastic scattering. For the study of sd-shell nuclei with the (d, t) and $(d, ^3$He$)$ reactions, energies near 20 MeV appear optimum. Hence we feel that the measurements and calculations as reported in the paper provide a new and powerful means for the evaluation of model wave functions.

VI. ACKNOWLEDGMENTS

We extend our appreciation to Dr. T. Tamura and Dr. T. Udagawa for supplying us with a copy of the computer code MARS and for several helpful conversations. We are indebted to Dr. B. H. Wildenthal for providing us with the results of his shell-model calculation. We also acknowledge many helpful discussions with Dr. W. J. Thompson. We thank Dr. E. J. Erskine for the use of the computer code BANDMIX.

---

†Work supported by the Atomic Energy Commission.

[1]J. Dubois, Nucl. Phys. A104, 657 (1967).
[2]R. L. Kozub, Phys. Rev. 172, 1078 (1968).
[3]H. H. Duhm, Nucl. Phys. A118, 563 (1968).
[4]J. M. Joyce, R. W. Zurmuhle, and C. M. Fou, Nucl. Phys. A132, 629 (1969).
[5]P. D. Kunz, E. Rost, and R. R. Johnson, Phys. Rev. 177, 1737 (1969).
[6]J. Dubois and L. G. Earwaker, Phys. Rev. 160, 925 (1967).
[7]A. R. Poletti, A. D. W. Jones, J. A. Becker, R. E. McDonald, and R. W. Nightingale, Phys. Rev. 184, 1130 (1969).
[8]A. R. Poletti, J. A. Becker, and R. E. McDonald, Phys. Rev. C 2, 964 (1970).
[9]L. C. Haun, N. R. Roberson, and D. R. Tilley, Nucl. Phys. A140, 333 (1970).
[10]H. J. Maier, J. G. Pronko, and C. Rolfs, Nucl. Phys. A146, 99 (1970).
[11]M. Arditi, L. Bimbot, H. Doubre, N. Frascaria, J. P. Garron, M. Riou, and D. Royer, Nucl. Phys. A165, 129 (1971).
[12]E. Kramer, G. Mairle, and G. Kaschl, Nucl. Phys. A165, 353 (1971).
[13]J. R. Powers, H. T. Fortune, R. Middleton, and O. Hansen, Phys. Rev. C 4, 2030 (1971).
[14]R. Engmann, F. Brandolini, I. Mauritzson, Nucl. Phys. A171, 418 (1971).
[15]R. A. Lindgren, R. G. Hirko, J. G. Pronko, A. J. Howard, M. W. Sachs, and D. A. Bromley, Nucl. Phys. A180, 1 (1972).
[16]G. G. Frank, M. W. Greene, D. T. Kelly, A. A. Pilt, and J. A. Kuehner, Phys. Rev. Letters 28, 571 (1972).
[17]J. B. McGrory and B. H. Wildenthal, Phys. Letters 34B, 373 (1971).
[18]T. Tamura, D. R. Bes, R. A. Broglia, and S. Landowne, Phys. Rev. Letters 25, 1507 (1970).
[19]J. M. Joyce, W. S. McEver, R. O. Nelson, R. V. Poore, and N. R. Roberson, Bull. Am. Phys. Soc. 15, 598 (1970).
[20]T. Tamura, Rev. Mod. Phys. 37, 679 (1965).
[21]S. K. Penny and G. R. Satchler, Nucl. Phys. 53 145 (1964).
[22]G. W. Schweimer and H. Rebel, des Zyklotron-Laboratoriums, 1970 (unpublished).
[23]T. Tamura, Oak Ridge National Laboratory Report No. 4152, 1967 (unpublished).
[24]H. R. E. Tjin A Djie, K. Mulder, F. Udo, A. Groenefeld, L. A. Ch. Loerts, A. D. Hill, and P. E. Hodgson, Nucl. Phys. A106, 85 (1968).
[25]T. Tamura, Nucl. Phys. 73, 241 (1965).
[26]M. P. Fricke and G. R. Stachler, Phys. Rev. 139, B567 (1965).
[27]T. Tamura, private communication.

[28]E. Rost, Phys. Rev. 154, 994 (1966).
[29]D. Dhenhard and J. L. Yntema, Phys. Rev. 160, 964 (1967).
[30]B. H. Wildenthal, private communication.
[31]F. Everling, Nucl. Phys. A115, 563 (1968).
[32]R. J. de Meijer, H. F. J. van Royen, and P. J. Brussaard, Nucl. Phys. A164, 11 (1971).

PHYSICAL REVIEW C VOLUME 6, NUMBER 6 DECEMBER 1972

Gamma Decay of States of ^{88}Y Excited by the ^{88}Sr$(p, n)^{88}$Y Reaction*

F. Gabbard, Gary Chenevert,† and K. K. Sekharan
Department of Physics and Astronomy, University of Kentucky, Lexington, Kentucky 40506
(Received 7 August 1972)

The ^{88}Sr$(p,n)^{88}$Y and ^{88}Sr$(p,n\gamma)^{88}$Y reactions have been used to study the excited states of ^{88}Y up to an excitation energy of 1832 keV. Determinations of the excitation energies of 18 levels to an accuracy of ±1 and ±2 keV, for levels with excitation energies less than and greater than 800 keV, respectively, have been made. Angular distributions of five γ rays deexciting states at 232, 393, 706, and 766 keV were measured and analyzed according to the statistical-model theory. This analysis confirms assignments of J^π values of 5^-, 1^+, 2^-, and 0^+ to these respective states. Of particular interest is the 2^- level at 706 keV. The intensities of neutrons from the ^{88}Sr$(p,n)^{88}$Y reaction exciting levels up to 1832 keV have been compared with statistical-model calculations of the neutron yields to the respective states for particular assumed spin values. Consistent spin-parity assignments are given for many of the levels observed.

I. INTRODUCTION

The levels in ^{88}Y have been studied in a number of experiments.[1-10] The principal components of the levels below an excitation energy of 2.5 MeV have been described in terms of particle-hole multiplets.[4,9,10] There is general agreement about the spin-parities of the ground state and the excited states at 232, 393, and 766 keV. There is still extensive confusion about the levels in the vicinity of 706 keV of excitation energy of ^{88}Y. There is evidence for a triplet of states near this energy[1,7,9,10] having spin-parities of 6^+ and/or 7^+ and 1^+, 2^- or a variety of other possibilities. Dutt and Gabbard[7] have observed excitation of the level(s) near 706 keV through the ^{88}Sr$(p,n)^{88}$Y reaction. Statistical-model analysis of the (p,n) data indicates $J^\pi = 2^-$ for the level observed. This analysis gives an unambiguous preference for the 2^- assignment. The energy resolution of the experiment was about 15 keV, leaving a question as to whether the neutron group observed excites a single level. Another problem concerns levels near 1250 keV of excitation in ^{88}Y.[9,10] There is disagreement as to the spin-parities of these states.

In an attempt to unravel this state of affairs, the γ decay of the low-lying states of ^{88}Y produced through the ^{88}Sr$(p, n\gamma)^{88}$Y reaction has been studied.

The (p, n) excitation of levels in ^{88}Y selectively populates low-spin states for which an orbital angular momentum transfer of less than five units is required. Levels with spins of 6 or higher are not expected to be observable.

The principal configurations of the low-lying states of ^{88}Y are expected to be proton-particle–neutron-hole states including $(p_{1/2}g_{9/2}^{-1})$, $(p_{1/2}p_{1/2}^{-1})$, $(p_{1/2}p_{3/2}^{-1})$, $(g_{9/2}g_{9/2}^{-1})$, $(g_{9/2}p_{1/2}^{-1})$, $(p_{1/2}f_{5/2}^{-1})$, $(g_{9/2}p_{3/2}^{-1})$, and $(g_{9/2}f_{5/2}^{-1})$, as described by Comfort and Schiffer.[10] There is also evidence from ^{86}Sr$(d, p)^{87}$Sr and ^{88}Sr$(p, d)^{87}$Sr for low-lying neutron states containing the neutron configuration $[\nu(1g_{9/2})^{-2}(2d_{5/2})]$.[1,11] Recent results of Holden, Kolata, and Daehnick[12] indicate configurations of the form $[\pi(2p_{1/2})\nu(1g_{9/2})^{-2}(2d_{5/2})]_{J^\pi=2^-}$ in the ground state of ^{86}Rb. Here, π designates a proton and ν designates a neutron. Therefore, it seems reasonable that the $[\pi(2p_{1/2})\nu(1g_{9/2})^{-2}(2d_{5/2})]$ would be present in ^{88}Y at relatively low excitation energy. The $[\pi(1g_{9/2})\nu(1f_{5/2}^{-1})]$ and the $[\pi(1f_{5/2})^{-1}\nu(1g_{9/2})^{-1}]$ might be expected to mix with this $[p_{1/2}(g_{9/2})^{-2}d_{5/2}]$ configuration in the formation of 2^- and 3^- states. Evidence for the $f_{5/2}$ proton-hole configuration in the ground state of ^{88}Sr has been given by Richard *et al.*[13]

The work reported here provides additional evidence that the level at 706 keV (Ref. 7) has a J^π of 2^- and provides information concerning higher